

## SESAR Engage KTN – PhD final report

|  |   |
|--|---|
| PhD title:                             | Detection, classification, identification and mitigation of GNSS signal degradations by means of machine learning |
| Candidate's name:                      | Evgenii MUNIN   |
| Lead supervisor's name:                | Nicolas COUELLAN  |
| Co-supervisor's name (if applicable):  | Antoine BLAIS   |
| Proponent institute:                   | ENAC laboratory   |
| Consortium institutes (if applicable): | -   |
| Thematic challenge:                    | N/A   |
| Edition date:                          | 25 July 2022  |
| Edition:                               | 1.0   |
| Dissemination level:                   | Public  |

The opinions expressed herein reflect the authors' views only. Under no circumstances shall the SESAR Joint Undertaking be responsible for any use that may be made of the information contained herein.



This project has received funding from the SESAR Joint Undertaking under the European Union's Horizon 2020 research and innovation programme under grant agreement No 783287.

## 1. Abstract

Among the navigation means, Global Navigation Satellites Systems (GNSS), and namely the Global Positioning System (GPS), have become essential and the availability of a GNSS navigation solution on board seems completely natural. However, the quality of the position calculated by the on-board equipment may be reduced when the received signal is degraded. This degradation can find its origin in a defect of the signal generation system, carried by the satellite, or in the receiving conditions, typically when interferences or multipaths are in addition to the desired signal.

The objectives of the thesis were to detect, classify, identify and finally reduce the impairments of the GNSS signals seen by the on-board receiver, by means of Machine Learning techniques.

More specifically, the performance of Machine Learning methods has been assessed on the signal at the correlator output, the correlator output in short. Indeed, the correlator output is a key element in the calculation of the aircraft's position by the receiver, and, consequently, it is the link in the signal processing chain where the degradations have the most significant impact.

Correlations of the received signal with a local replica over a (Doppler shift, propagation delay)-grid are mapped into grayscale 2D images. They depict the received information possibly contaminated by multipath propagation. The images feed a Convolutional Neural Network (CNN) for automatic feature construction and multipath pattern detection.

The issue of unavailability of a large amount of supervised data required for CNN training has been overcome by the development of a synthetic data generator. It implements a well-established and documented theoretical model. A comparison of synthetic data with real samples is proposed.

The complete framework is tested for various signal characteristics and algorithm parameters. The prediction accuracy does not fall below 93% for Carrier-to-Noise ratio (C/N<sub>0</sub>) as low as 36 dBHz, corresponding to poor receiving conditions. In addition, the model turns out to be robust to the reduction of image resolution.

## 2. Objective of the study

The objectives of the thesis were to detect, classify, identify and finally reduce the impairments of the GNSS signals by means of Machine Learning techniques applied to the signal at the output of the correlator.

More specifically, in a first step, the correlator output in presence of known degradations had been modelled, to enable the training phase of the Machine learning algorithms on a reference dataset. These algorithms had to be identified or designed and implemented during the thesis. In a second step, the Machine Learning algorithms were then to be run on a validation dataset to detect, classify and identify the different degradations. Depending on the performance achievements, methods aiming at mitigating the effect of the degradations could be implemented in a last step. These methods may range from a simple exclusion of a degraded signal from the calculation of the position solution to methods as fine as cancellation of the anomaly by means of techniques similar to the ones used in the suppression of the pollution noise in acoustics.

## 3. Motivation

The constant growth of air traffic requires the continuous improvement of the Air Traffic Management (ATM) system and in particular of the supporting services such as Communication, Navigation and Surveillance (CNS).

Indeed, the necessary increase of the capacity of the ATM system can not be done without better performances of the CNS components. More specifically, the navigation performances of the aircraft, accuracy, integrity, continuity and availability, have to be strengthened. Among the navigation means, GNSS, and especially GPS, have become essential and the availability of a GNSS navigation solution on board seems completely natural.

However, the quality of the position calculated by the on-board equipment may be reduced when the received signal is degraded. This degradation can find its origin in a defect of the signal generation system, carried by the satellite, it is the evil waveform case, or in the receiving conditions, typically when interferences or multipaths are in addition to the useful signal.

Inside the GNSS receiver, the signal at the correlator output, the correlator output in short, is a key element in the calculation of the aircraft's position and consequently is the link in the signal processing chain where the degradations have the most significant impact. That is why large amounts of research and analysis have been conducted to detect, classify, identify and finally mitigate the degradations at the correlator output.

They have clearly shown the limits of the "classical" signal processing methods, proposing solutions whose effectiveness is mixed.

The recent and significant advances in Artificial Intelligence (AI), and notably in Machine Learning, have opened up new perspectives, and the question arises if these techniques could provide a significant reduction of the impact of the signal degradations on the quality of the position delivered to the aircraft navigation system.

#### 4. Advances this work has provided with regard to the state of the art

A large amount of research and analysis has been conducted so far to detect, classify, identify and finally mitigate these impairments. As the GNSS receiver has to track the direct signal by mean of a Delay-Locked Loop (DLL) to estimate the propagation delay, multiple methods have been proposed which use the already existing correlator outputs required by this DLL. The narrow correlator technique [1], the early-late-slope technique [2], the strobe correlator [3], the double-delta correlator [4] and the multipath intensive delay lock loop [5] are among the most representative methods of this class. They all take advantage of the geometric shape of the auto-correlation function of the Pseudo-Random Noise (PRN) code, as defined later on in (2) and (3) and illustrated in Figure 3, to detect and mitigate the multipath distortion. Their relative simplicity is their principal benefit at the expense of their effectiveness. On the other hand, more sophisticated techniques, yet demanding in hardware resources, have been developed. In the statistical approach, the Multipath Estimating Delay Locked-Loop (MEDLL) is a reference implementation of the maximum likelihood principle [6]. It matches the correlator outputs with candidates of multipath auto-correlation functions parameterized by magnitudes, delays, and phases. The shortest estimated delay is then retained as the one of the direct path. The frequency domain has also been explored, through the Fourier transform [7] or the wavelet decomposition [8]. Indeed, due to their specific spectral characteristics in comparison to the direct path, the multipath can be identified and excised. However, these methods may damage the signal of interest, especially when the multipath frequencies are close to the spectrum of the direct path.

To overcome the limitations of these classical signal processing methods, Machine Learning techniques have also been considered. Starting from the early 2000s, some research work has been dedicated to the use of Machine Learning techniques to facilitate the error mitigation in GNSS signals. For instance, a hybrid neural network architecture based on multilayer perceptron to mitigate multipath error for Low Earth Orbit (LEO) satellites has been proposed [9]. Later, with the

advances of kernel methods, the authors of [10] were able to develop a support vector regressor to mitigate multipath on ground fixed GPS stations and using signal geometrical features. Other similar studies were conducted with various choices of features construction.

For example, in [11, 12], non-line of sight (NLOS) multipath detection is carried out using features directly extracted from the correlator output. The recent and significant advances in Artificial Intelligence, and notably in Machine Learning, have opened up new perspectives. In [13], using a CNN, a carrier-phase multipath detection model is developed. The authors propose to extract feature map from multi-variable time series at the output of the signal processing stage using 1-dimensional convolutional layers. Deep learning spoofing attack detection in GNSS systems was addressed in the research literature [14] as well. Hand-crafted features based on early-late phase, delay and signal level from the correlation output of the tracking loop were used to train a deep fully-connected neural model. A review of the recent applications of Machine Learning in GNSS is also proposed in [15], focusing on use cases relevant to the GNSS community.

The method proposed in this PhD thesis aims at making use of an efficient CNN architecture for multipath detection. The intent is to exploit the full power of CNN by letting the convolutional mechanism construct its own feature space from the whole correlator information.

Indeed, features are not extracted from the signal but the signal is rather transformed into 2D images in the time–frequency domain. No correlator output signal information is lost during the process and the CNN is able to build its own representation of corrupted/non corrupted correlated signals.

The search ranges for the values of the propagation delay and the Doppler shift spans a 2D grid which forms in turn 2D-images at the output of the correlation process, the correlator output in short. Regarding the phase value, the phase estimation error is captured over  $[0, 2\pi]$  by mean of two orthogonal projections. These projections are carried out by the correlation with the In-phase (I) signal replica on one side and the in-Quadrature (Q) signal on the other. A diagram representing this process is given in Figure 1. As depicted, the correlation operation is implemented through a product followed by an integrate and dump stage and generates 2D image representations of the I and Q channels. These images coded into 3D tensors will feed a downstream CNN, as it will be seen below.

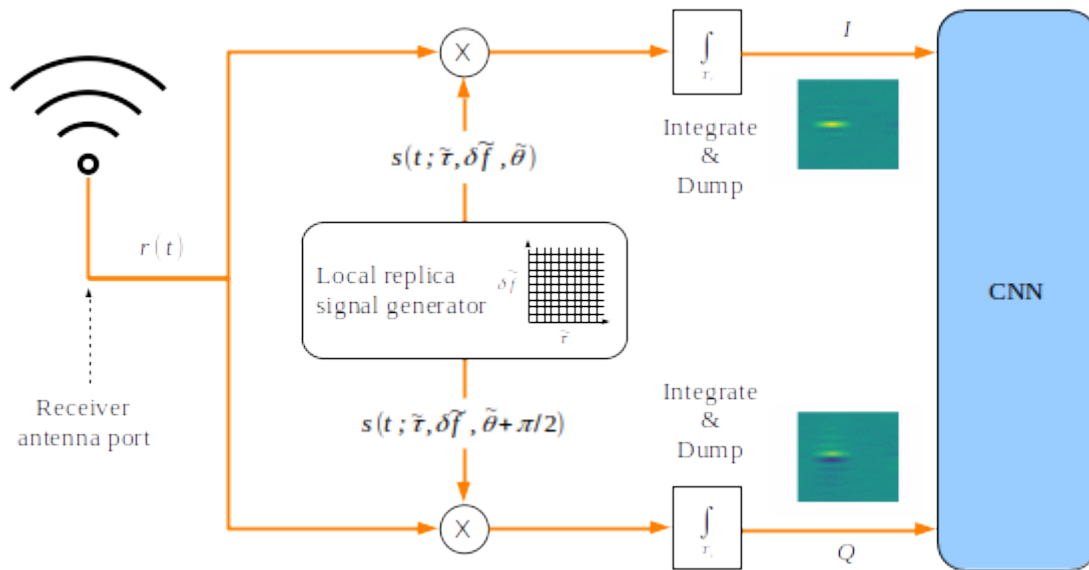


Figure 1: Synoptic view of the correlation process. The received signal is correlated with two local replica signals in quadrature whose parameters span a grid. The two correlator outputs form then 2D-images which fed a downstream CNN. The tilde notation indicates the local parameter by opposition to the received signal unknown parameter.

This PhD thesis proposes a complete framework to train and assess a CNN model on correlator output 2D-images in order to detect whether the GNSS signal is subject to multipath or not. A graphical representation of this framework is given in Figure 2. The developed technique exploits the full power of deep learning architectures by sampling the complete correlated signal information in the time–frequency domain and the I and Q channels. Features are not handcrafted but rather constructed automatically by the convolution mechanism that elaborates its own representation of

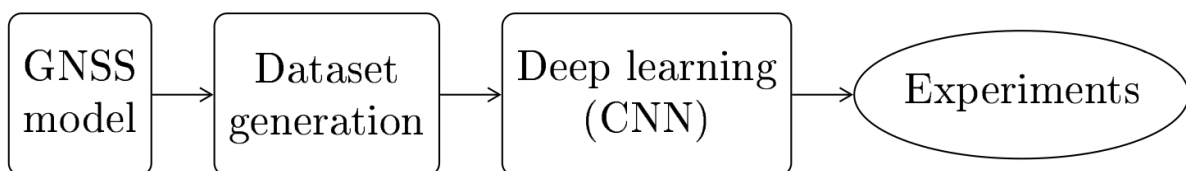


Figure 2: Proposed framework to train and assess a CNN model on correlator output 2D-images.

the relevant feature space to detect multipath corrupted signals.

The main contributions of this PhD thesis can be listed as follows:

- Raw and complete information from the GNSS correlator outputs are synthesized in 2D-images. The correlation delay and Doppler shift ranges are selected in order to capture complete multipath information. This is a novel approach in comparison to standard multipath mitigation techniques that are using only one dimensional delay correlation information.
- A CNN model is used to automatically extract relevant features for multipath detection from the images of correlator outputs. This contributes to the very recent and emergent use of modern Machine Learning techniques in the GNSS signal processing field.

- The proposed framework covers the generation of image data, the choice of the CNN architecture, its training as well as its validation. Experiments are fully reproducible. To the best of our knowledge such complete workbench is unique in the research community.
- The achieved average detection accuracy for realistic multipath parameters ranges in standard receiving conditions is above 93%. This performance has been shown to be robust to the reduction of correlator output image resolution.

## 5. Methodology

### 5.1 GNSS signal model

The fundamental principle behind the calculation of the user position by a GNSS receiver is trilateration. It implies the measurement of the geometric distances between the antenna of the receiver and satellites of known positions. Indeed, a distance  $d$  in particular is estimated through the propagation delay affecting the signal during its propagation from the satellite to the receiver antenna,  $\tau = d/c$  with  $c$  the speed of light. This is made possible by a specific signal structure, recalled in Equation (1) which models the signal at the antenna port [16]:

$$r(t) = 2CD(t - \tau)c(t - \tau) \cos(2\pi(f_c + \delta f)t + \theta) + b(t) \quad (1)$$

where

- $C$  is the power of the received signal,
- $D(t)$  is the navigation message, binary encoded ( $\pm 1$ ),
- $c(t)$  is the PRN code sequence, specific to each satellite,
- $f_c$  is the carrier frequency,
- $b(t)$  is an Additive White Gaussian Noise (AWGN) which accounts for the thermal noise of the receiver, referred to the antenna port.

The results presented in this PhD thesis were established using the PRN code sequences of the GPS L1 C/A legacy signal. However, the authors are confident that they could be generalized to other navigation signals, with the same structure, as no specific assumption has been made on  $c(t)$ .

In this model, the receiving condition of a signal in particular is assessed by its  $C/N_0$  figure, in other words the ratio of the signal power to the Power Spectral Density (PSD) level  $N_0$  of the (white) noise  $b(t)$ . Clearly, the accuracy of the estimation of the related distance  $d$  will depend upon this  $C/N_0$  ratio. Without any other perturbation than the noise, the quality of the final position calculated by the receiver, from a set of distances  $d$  at its disposal, is then completely determined by the corresponding set of  $C/N_0$  ratios, along with the relative satellites–receiver geometry though.

A model of the I and Q correlator outputs [16] is as follows:

$$I = AK(\Delta\tau) \cos(\pi\Delta f T_i + \Delta\theta) \text{sinc}(\pi\Delta f T_i) + n_I \quad (2)$$

$$Q = -AK(\Delta\tau) \sin(\pi\Delta f T_i + \Delta\theta) \text{sinc}(\pi\Delta f T_i) + n_Q \quad (3)$$

with

- $T_i$  the integration time,
- $A$  a coefficient depending on  $C$ ,  $D$  and  $T_i$ ,
- $\Delta\tau$  the propagation delay estimation error,
- $\Delta f$  the Doppler shift estimation error,
- $\Delta\theta$  the phase estimation error,
- $K(\Delta\tau)$  the auto-correlation function of the PRN code in  $\Delta\tau$ ,

- $n_I$  and  $n_Q$  the noise components.

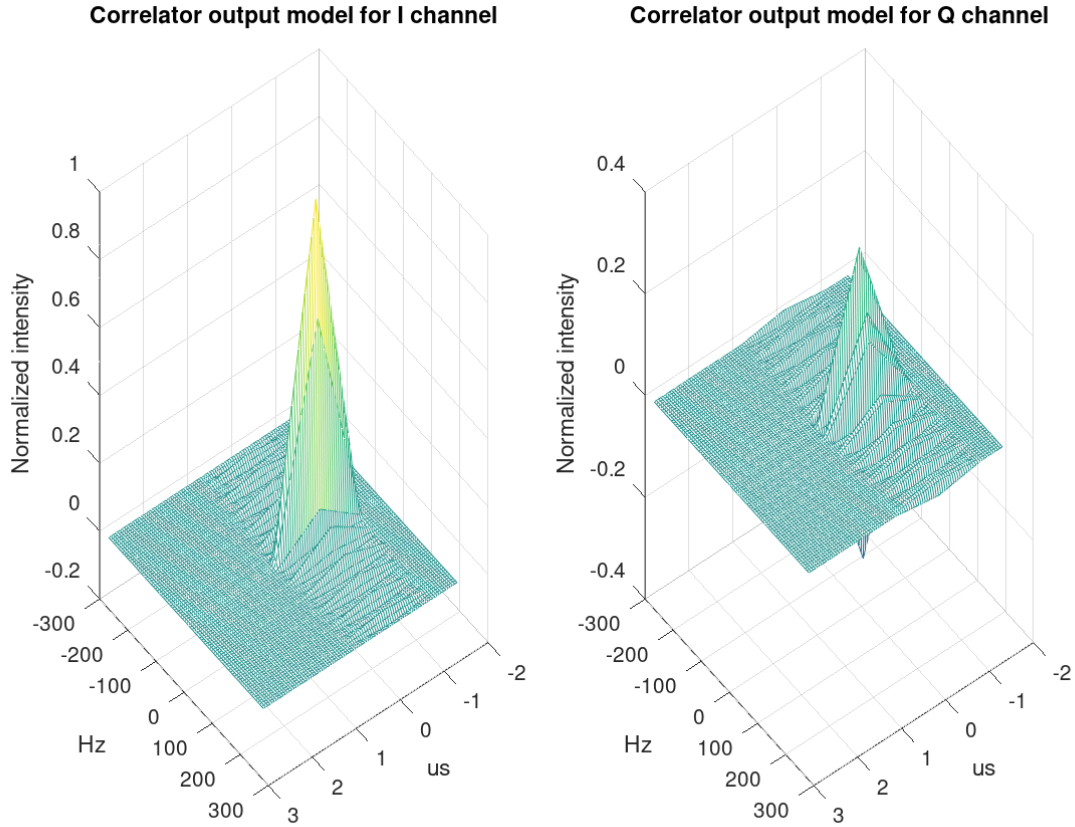


Figure 3: An illustration of the noise-free  $I$  and  $Q$  correlator output model,  $\Delta\theta$  set to 0, PRN number to 1.

Figure 3 gives a graphical representation of the noise-free  $I$  and  $Q$  correlator outputs as functions of  $\Delta\tau$  and  $\Delta f$ , for  $\Delta\theta = 0$ .

## 5.2 Multipath contamination

As some perturbations can distort the desired signal, the received signal cannot always be modelled simply using Equation (1). Among these perturbations, multipath is considered to be an important source of degradation [17]. This is especially the case in urban environment, inducing reduced positioning accuracy. Multipath is due to the reflection of the direct signal path on a surface in view of the receiver. As a consequence, a specific multipath can be modelled in the same way as the direct signal in (1):

$$m(t) = 2C_{MP} D(t - \tau_{MP})c(t - \tau_{MP}) \cos(2\pi(f_c + \delta f_{MP})t + \theta_{MP}) \quad (4)$$

where  $C_{MP}$ ,  $\tau_{MP}$ ,  $\delta f_{MP}$  and  $\theta_{MP}$  have the same definition as in Section 5.1, but for the multipath.

Due to the larger propagation distance of the multipath in particular, it is to be noted that  $C_{MP} \leq C$  and  $\tau_{MP} > \tau$ . What is more, depending on the time-varying relative geometry of the satellite–receiver–reflector system, there is no reason for  $\delta f_{MP}$  being equal to  $\delta f$  nor  $\theta_{MP}$  having the same value as  $\theta$ .

In general, a receiver is impacted by multiple multipaths, especially in urban environments where reflectors are numerous. Sometimes, the direct path may even be absent due to an obstruction, for example when high buildings are surrounding the receiver [18]. However, in this study the assumption is made that the direct path is always present and a single multipath will be considered.

## 5.3 Convolutional neural network model

### Image classification using CNN

Convolutional neural networks [20] are nowadays considered as among the most powerful tools to learn information from images. This is explained by their computational efficiency and their impressive performance on image information processing. Their learning capability comes from their ability to automatically construct and combine abstract features from an image. The first layers of the network are composed of convolutional layers. Such layers apply several filters over the various regions of the input image and create feature maps that are various versions of the filtered input image. Several convolutional layers are usually stacked in order to progressively extract meaningful information from the feature maps as the depth of the network is increased. The last layers of the CNN perform the task of classification usually through several layers of neurons with dense connectivity. The weights of each convolution layer filters (also called kernels) and those of the dense layers are learned through supervised learning based on gradient back-propagation. The underlying structure of convolutional layers has the advantage of having sparse connectivity and high weight sharing among neurons, which leads to much greater computational efficiency over fully connected neural networks when image sizes are large or the image resolutions are high.

The above principles are at the heart of CNN architectures. Several additional components are usually integrated in the network. Some Pooling layers are used in order to reduce the dimension of feature maps. A Flatten layer is added in front of the stack of dense layers so as to transform feature map information in vector-like input. To increase the generalization power of the network, a dropout mechanism can also be used to artificially and randomly remove a small portion of the neuron connection within the network. The number and the organization of these various components generate several possible CNN architectures [21].

### Choice of a CNN architecture

Among CNN architectures that have proven to be effective in practice [22], the Visual Geometry Group (VGG)-like architecture has been shown to be one of the best choice for image feature extraction [23]. Despite its number of parameters to be trained compared to other popular and more complex architectures such as Inception V3 [24], ResNet [25] and other variants, it has been widely adopted in practice by the Machine Learning community. The architecture is composed of several blocks of convolutional layers that are each separated by a pooling layer that decreases the feature map dimension between blocks. As the depth increases, the dimension of layer input decreases but the number of filters increases. When data are organized on a multi-scale basis, mixing macro and micro patterns, the number of convolutional blocks should be chosen sufficiently large. For the GNSS multipath application, such multi-scale representation is not expected in the signal. This is the reason why the chosen architecture only includes one convolutional block composed of two convolutional layers. It is therefore a very simple instance of a VGG-like network. VGG architectures are usually implemented for RGB images (meaning three input channels: the 'R', 'G' and 'B' channels). For the specific case of I/Q images, each input image is actually composed of two channels (I channel + Q channel) that are sharing the GNSS correlation signal information. Input images are therefore tensors of size  $N \times N$  and depth 2. Figure 4 provides the precise network architecture and layer dimension used in this PhD thesis.

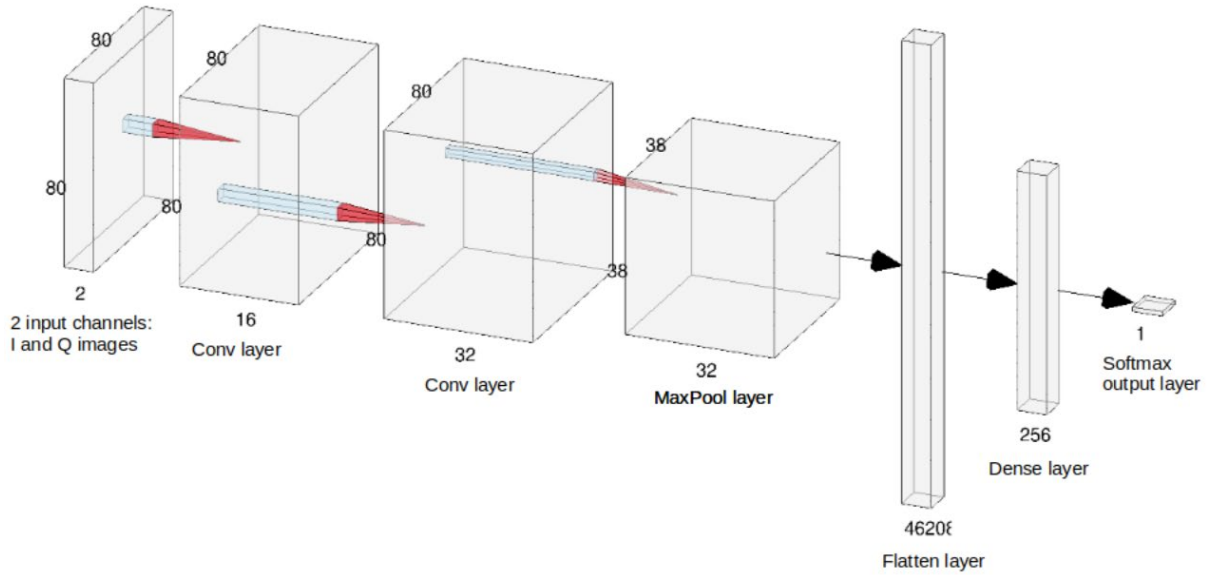


Figure 4: The CNN architecture used in this PhD thesis: the input has 2 channels corresponding to I and Q channels, the first and second convolutional layers have 16 and 32 filters respectively with ReLu activations and the pooling layer is a  $2 \times 2$  max pooling operation layer (this figure has been generated by the NN-SVG tool (LeNail, 2019)).

## 6. Description of the data the study relies on

In order to test our prediction models, an artificial signal generator was developed. The data are generated in the form of two matrices, one for each of the I and Q channels, according to Equations (2) and (3). The axes of these matrices are in Doppler shift estimation error  $\Delta f$  and code delay estimation error  $\Delta \tau$ . The output data corresponding to this main signal can be parameterized as a function of the coherent integration time  $T_i$  in ms and the carrier-to-noise ratio  $C/N_0$  in dBHz.

### 6.1 Noise sample production

At the correlator output the noise is not only spatially correlated inside each I and Q image, but also cross-correlated between them. The exact derivation of the auto-correlation and cross-correlation functions of the noise are still to establish. To overcome this impossibility to generate the noise contribution at the correlator output from an analytical model, a workaround has been developed. A signal  $r(t)$  (1) made of a simple noise term  $b(t)$  is correlated according to the process described in Figure 1, as would be a true received signal. This correlation process is implemented in a software GNSS receiver developed by the SIGnal processing and NAVigation (SIGNAV) research team of the ENAC laboratory. The noise samples available at the correlator output are then collected and stored in a dataset, to be added on demand as  $n_I$  and  $n_Q$  in Equations (2) and (3). Figure 5 gives an example of empirical auto-correlation and cross-correlation functions of noise samples for PRN number 10.

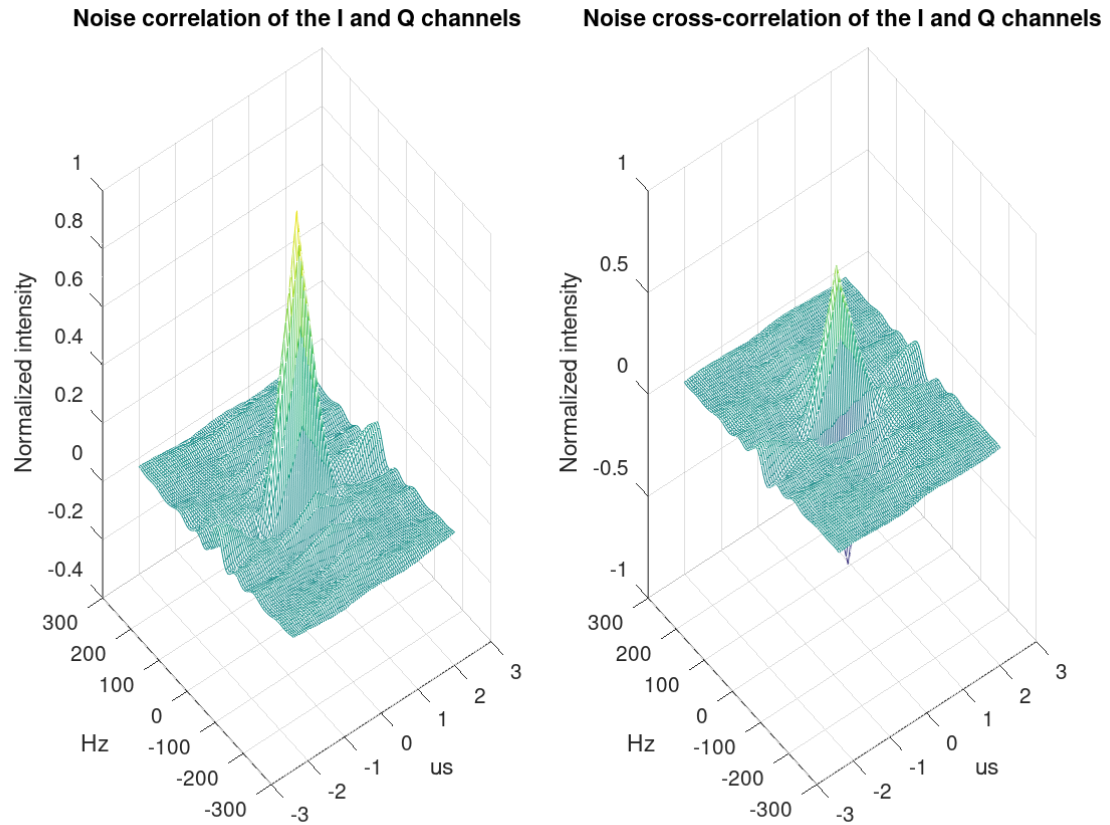


Figure 5: Empirical auto-correlation and cross-correlation functions of the noise at the correlator output for the I and Q channels, PRN number set to 10.

An illustration of the noisy output of the synthetic data generator for  $T_i = 20$  ms and  $C/N_0 = 45$  dBHz is given in Figure 6, with the corresponding flattened images in Figure 7 (note the value of the navigation bit  $D = -1$  this time, in comparison to Figure 3 where  $D = +1$ ).

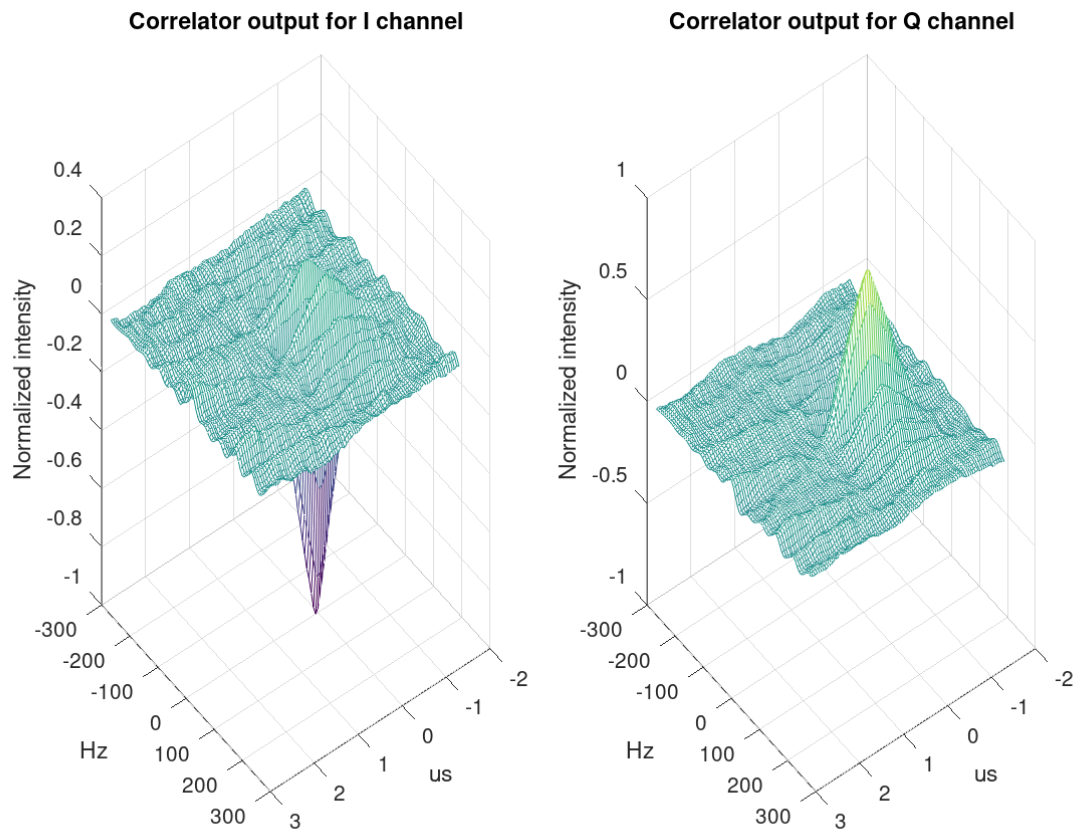


Figure 6: An illustration of the I and Q correlator outputs of the synthetic data generator, PRN number set to 1.

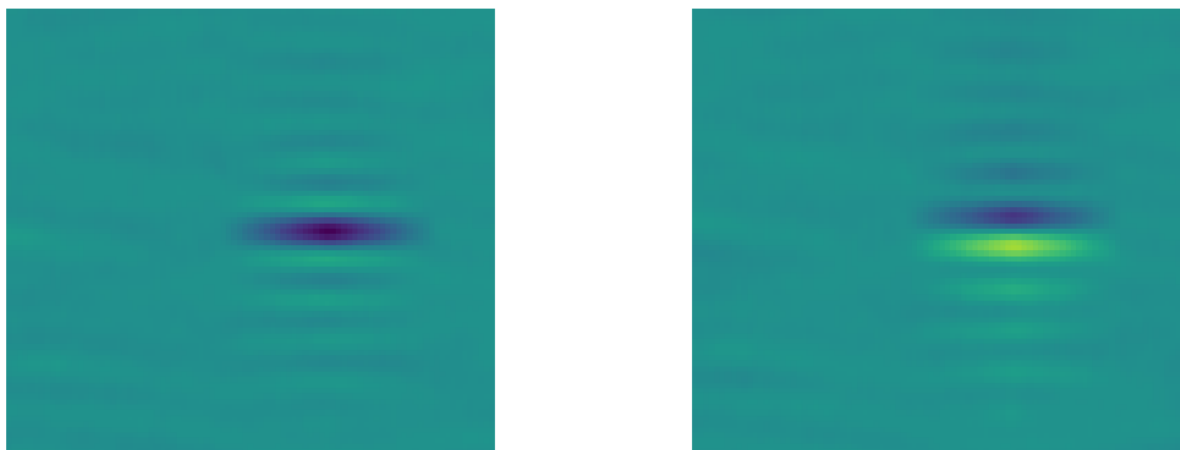


Figure 7: The I and Q correlator outputs of the synthetic data generator as images, PRN number set to 1

## 6.2 Assessment of the synthetic data

In order to validate the synthetic data generator its outputs have been compared to the data from an IFEN SX3 GNSS receiver. Two different data collection sessions have been conducted.

- 1 The receiver has been fed with a signal produced by a Spirent GSS6560 generator. The scenario implemented in the generator simulates the take-off and initial climb of a commercial aircraft from runway 14L of the Toulouse–Blagnac Airport. The flight happens on Tuesday the 28<sup>th</sup> of May 2019 from 12:55 UTC. The multipaths are disabled in this scenario.
- 2 A high end GNSS antenna has been connected to the receiver. The antenna was set up in a clear view site to avoid multipath contamination. Moreover, only signals from high elevation satellites were considered afterwards so that the collected samples could be considered as multipath free. The recording was carried out on Friday the 14<sup>th</sup> of February 2000 from 08:05 UTC.

In both cases the SX3 receiver sampling frequency was set to 20 MHz. The samples were stored for post-processing by the software GNSS receiver already mentioned in Section 6.1. The resulting reference images are available on [19] for the two sessions. Figures 8 and 9 provide an example of visual comparison of images. It is worth noting that these real data were used only to validate the generator. Indeed, for training purposes it would be unrealistic to produce a sufficient amount of labelled physical signals.

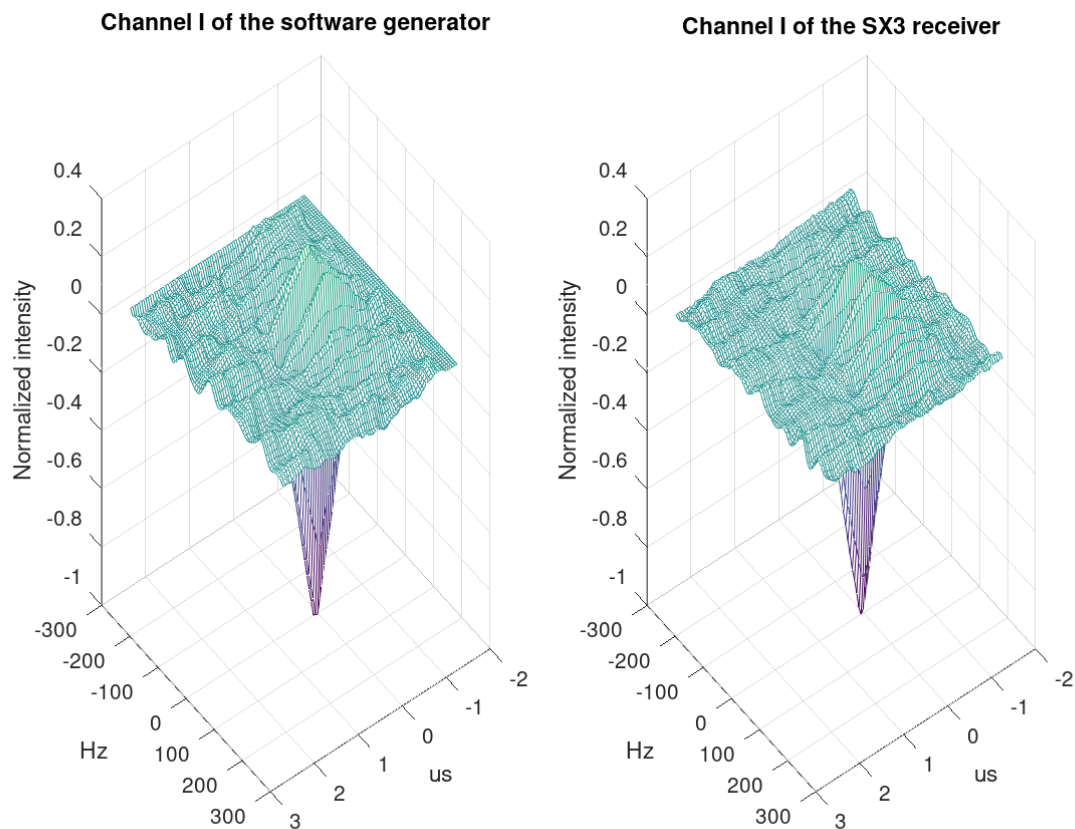


Figure 8: Comparison between an output of the synthetic data generator and a real sample from a SX3 receiver, I channel, PRN number set to 1

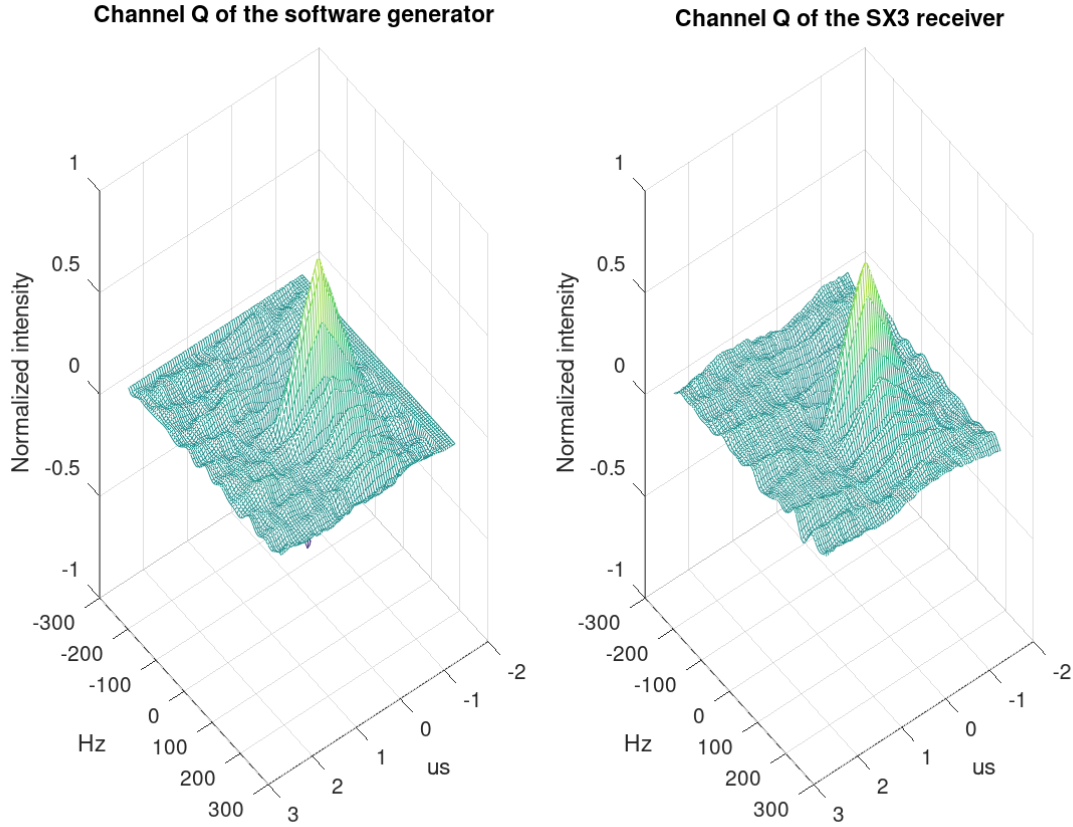


Figure 9: Comparison between an output of the synthetic data generator and a real sample from a SX3 receiver, Q channel, PRN number set to 1

### 6.3 Model for GNSS multipath data generation

The considered model integrates I and Q signals, I and Q multipath and correlated receiver noise. If a multipath signal is received in addition to the main signal, as the signal processing chain is linear, the correlator output can then be considered as the sum of the correlator output of the main signal and the one due to the multipath. In this work, a single multipath contamination is considered. Its contribution ( $I_{MP}$ ,  $Q_{MP}$ ) to the correlator output is considered as an additional term to the main signal ( $I$ ,  $Q$ ), detailed in (2) and (3):

$$I' = I + I_{MP}(\alpha_{MP}, \Delta\tau_{MP}, \Delta f_{MP}, \Delta\theta_{MP}) \quad (5)$$

$$Q' = Q + Q_{MP}(\alpha_{MP}, \Delta\tau_{MP}, \Delta f_{MP}, \Delta\theta_{MP}) \quad (6)$$

where

- $\alpha_{MP} = C_{MP}/C < 1$  is the multipath attenuation coefficient in comparison to the main path,
- $\Delta\tau_{MP} = \tau_{MP} - \tau > 0$  is the code delay in excess to the main signal delay,
- $\Delta f_{MP} = \delta f_{MP} - \delta f$  is the difference between the Doppler shift of the main signal and the multipath,
- $\Delta\theta_{MP} = \theta_{MP} - \theta$  is the difference between the phase of the main signal and the multipath.

### 6.4 The I/Q image dataset generation

The data generator has been implemented with the Python language [19] to produce datasets of I and Q images according to the signal and noise models detailed in Sections 6.1 and 6.3. This

software is referred as the generator in this paper. The generator is fully configurable with respect to the following parameters:  $\alpha_{MP}$ ,  $\Delta\tau_{MP}$ ,  $\Delta f_{MP}$  and  $\Delta\theta_{MP}$  which entirely define the multipath. Their probability distributions are clarified in Section 7 dedicated to the experiments conducted with the help of the generator,

- $C/N0$  ratio which sets the strength of the direct path signal with respect to the receiver noise,
- $N$  the number of pixels along each of the delay and Doppler shift axes. The size of the images is then  $N \times N$  pixels. It is important to mention that  $2N^2$  is then the number of correlators required to implement the technique proposed in this PhD thesis. Hence, it is a direct measure of its complexity as the correlation operation is from far the most power and time consuming process in a GNSS receiver,
- $T_i$  the coherent integration time. In this study  $T_i = 20$  ms, a value corresponding to the duration of one navigation bit  $D$  as defined in Equation (1). It ensures the longest correlation time, so the best accuracy for  $\tau$ ,  $\delta f$  and  $\theta$  estimation, without bit transition during the correlation which would otherwise lower the final result.

The experiments led in this work were all done with datasets of 600 pairs of I and Q images, equally split in 300 with multipath and 300 without. However, the generator can provide datasets of arbitrary size and distribution on demand.

## 7. Computational experiments

This section describes the experiments which were conducted to evaluate the performance of the proposed model on the dataset described in Section 6.4. For each test case the mean, median and standard deviation values of accuracy and F1 score averaged over 20 runs are provided. The range and probability distribution of the multipath parameters as defined in Equations (5) and (6) are set, unless otherwise specified, as follows:

- $\alpha_{MP}$  the multipath attenuation coefficient is uniformly distributed in  $[0.1, 0.9]$ ,
- $\Delta\tau_{MP}$  the additional propagation delay of the multipath is also uniformly distributed, in  $[0, 3T_c/2]$ ,
- $\Delta f_{MP}$  the difference in Doppler shift between the direct signal and the multipath is distributed in  $[-125, +125]$  Hz according to a truncated zero-mean normal distribution with a standard deviation set to  $125/3$ ,
- $\Delta\theta_{MP}$  the difference between the phase of the main signal and the multipath is uniformly distributed in  $[0, 2\pi]$ ,
- The value of the navigation bit  $D$ , as defined in Equation (1), is chosen randomly with equal probability between  $-1$  and  $+1$  for each pair of I and Q images.

### 7.1. Influence of multipath characteristics

In these experiments the influence of the multipath characteristics on the detection performance is assessed. The experimental conditions are set in this way:  $C/N0 = 47$  dBHz and the image resolution is  $80 \times 80$ . This corresponds to good observation conditions for the direct path, so that the CNN response can be clearly observed. The tests were conducted on 5 equally spaced values for both the difference in Doppler shift  $\Delta f_{MP}$  from 0 to 50 Hz and the additional propagation delay of the multipath  $\Delta\tau_{MP}$  from 0 to  $T_c$ .

## 7.2. Influence of the signal to noise ratio C/N0

In these experiments the influence of  $C/N0$  ratio on the detection performance is assessed. The experimental conditions are the following:  $T_i = 20$  ms and the image resolution is  $80 \times 80$ . The multipath parameters distributions are identical to those defined in Section 5.2. The tests were conducted on equally spaced values of  $C/N0$  ratio from 24 to 46 dBHz.

## 7.3. Influence of the I/Q image resolution

In order to evaluate the performance of the multipath detector, the proposed algorithm was applied on images of various resolutions  $N \in \{20, 40, 60, 80\}$  with the intent to estimate the best compromise performance vs image resolution. The multipath parameters distributions are the same as before.

# 8. Results

## 8.1. Influence of multipath characteristics

The results are represented in Tables 1 and 2. They show that there is no significant influence of the Doppler shift on the detector performance. On the other hand, when the propagation delay approaches  $0.2T_c$  (meaning that the multipath gets close to the main signal), a slight degradation of the accuracy and F1-score by 6% can be observed.

Table 1: Mean ( $\mu$ ) and standard deviation ( $\sigma$ ) of prediction accuracy and F1-score with respect to Doppler shift.

| $\Delta f_{dop}$ (Hz) | 0    | 10   | 20   | 30   | 40   | 50   |
|-----------------------|------|------|------|------|------|------|
| $\mu_{Acc}$           | 0.97 | 0.96 | 0.96 | 0.98 | 0.97 | 0.99 |
| $\sigma_{Acc}$        | 0.01 | 0.01 | 0.02 | 0.02 | 0.01 | 0.01 |
| $\mu_{F1}$            | 0.96 | 0.99 | 0.97 | 0.97 | 0.97 | 0.99 |
| $\sigma_{F1}$         | 0.01 | 0.02 | 0.02 | 0.03 | 0.02 | 0.01 |

Table 2: Mean ( $\mu$ ) and standard deviation ( $\sigma$ ) of prediction accuracy and F1-score with respect to propagation delay.

| $\Delta\tau$ ( $T_c$ ) | 0.2   | 0.4   | 0.6   | 0.8   | 1.0 |
|------------------------|-------|-------|-------|-------|-----|
| $\mu_{Acc}$            | 0.94  | 0.94  | 0.98  | 0.96  | 1.0 |
| $\sigma_{Acc}$         | 0.01  | 0.023 | 0.022 | 0.012 | 0.0 |
| $\mu_{F1}$             | 0.94  | 0.95  | 0.98  | 0.95  | 1.0 |
| $\sigma_{F1}$          | 0.008 | 0.02  | 0.023 | 0.011 | 0.0 |

## 8.2. Influence of the signal to noise ratio C/N0

The results are presented on Table 3. From these results the current model shows high robustness towards the noisy incoming images for values down to 36–38 dBHz. Then, as expected, the model

performance decreases greatly with the value of the  $C/N0$  (when I and Q images are noisier). On Figure 10, it can be also observed that the standard deviation of the metrics decreases when the image becomes less noisy. This means that the detection model achieves greater robustness in performance when the noise decreases. A value of around  $C/N0 = 36$  dBHz seems to be also a threshold after which the performance is much higher.

Table 3: Mean ( $\mu$ ) and standard deviation ( $\sigma$ ) of prediction accuracy and F1-score with respect to carrier to noise ratio.

| $C/N0$ (dBHz)  | 24   | 26   | 28   | 30   | 32   | 34   |
|----------------|------|------|------|------|------|------|
| $\mu_{Acc}$    | 0.60 | 0.74 | 0.64 | 0.80 | 0.83 | 0.85 |
| $\sigma_{Acc}$ | 0.08 | 0.05 | 0.03 | 0.02 | 0.04 | 0.03 |
| $\mu_{F1}$     | 0.59 | 0.63 | 0.74 | 0.81 | 0.84 | 0.84 |
| $\sigma_{F1}$  | 0.08 | 0.08 | 0.04 | 0.02 | 0.03 | 0.02 |
| $C/N0$ (dBHz)  | 36   | 38   | 40   | 42   | 44   | 46   |
| $\mu_{Acc}$    | 0.93 | 0.97 | 0.98 | 0.96 | 0.97 | 0.97 |
| $\sigma_{Acc}$ | 0.02 | 0.02 | 0.01 | 0.03 | 0.01 | 0.02 |
| $\mu_{F1}$     | 0.89 | 0.97 | 0.97 | 0.96 | 0.98 | 0.97 |
| $\sigma_{F1}$  | 0.03 | 0.02 | 0.02 | 0.01 | 0.01 | 0.02 |

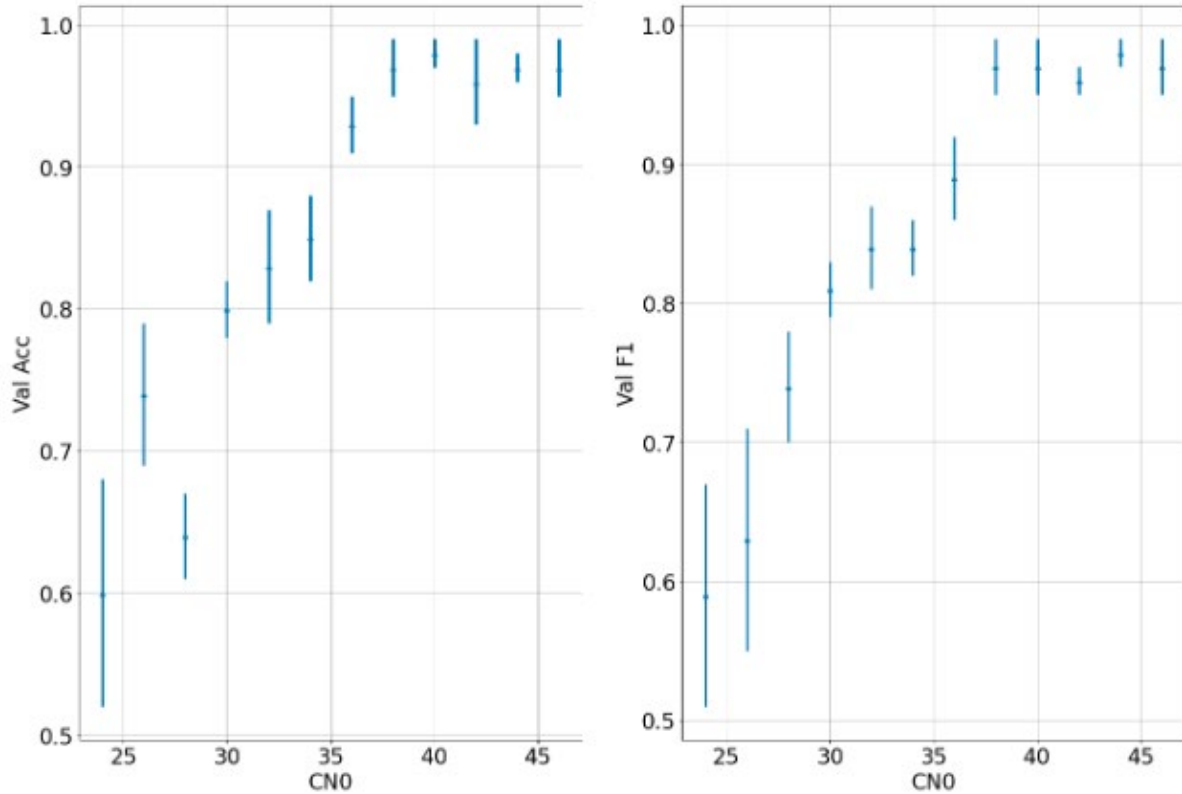


Figure 10: Average validation accuracy (left) and average F1 score (right) with respect to carrier to noise ratio C/N0 (vertical bars represent standard deviation values).

### 8.3. Influence of the I/Q image resolution

The results in Table 4 show that the model performance decreases with the image resolution. However, for resolutions above 40 pixels per axes, the model classification performance stays above 95%.

Table 4: Mean ( $\mu$ ) and standard deviation ( $\sigma$ ) of prediction accuracy and F1-score with respect to image resolution.

| Resolution (pixel) | 20   | 40   | 60   | 80   |
|--------------------|------|------|------|------|
| $\mu_{Acc}$        | 0.93 | 0.95 | 0.97 | 0.99 |
| $\sigma_{Acc}$     | 0.02 | 0.01 | 0.01 | 0.01 |
| $\mu_{F1}$         | 0.92 | 0.95 | 0.98 | 1.0  |
| $\sigma_{F1}$      | 0.02 | 0.01 | 0.01 | 0.0  |

## 9. Analysis of the results

The experiments exposed in section 8 put in light that the performance of the proposed method is more than adequate in the three axes of importance in our study:

- The multipath parameters have been varied over their respective realistic range to assess the validation accuracy. It is not less than 94% in any case,
- The  $C/N_0$  ratio, that reports the receiving condition of the GNSS signal of interest, was changed from 46 (good) to 24 (poor) dBHz,
- A failover is observed in the performance around 36 (fairly poor) dBHz, which establishes a quite acceptable operational limit to our network,
- The image resolution, parameterized by  $N$  the number of points per axes, has been gradually decreased to measure the robustness of the algorithm to hardware limitations. Indeed, a validation accuracy of 93% is still achieved for  $N = 20$ .

With respect to the chosen architecture, the experiments confirm that the detection task at hand does not require large depth as not much multi-scale learning seems to be needed. Indeed, our choice of a quite shallow architecture has proven to be appropriate for efficient multipath detection.

## 10. Conclusions and look ahead

In this PhD thesis, a complete GNSS multipath detection framework based on deep learning has been presented. The proposed method starts with the construction of training image data from synthetic receiver correlation outputs. A precise image generation process based on specific parameter definition intervals is described. This process optimizes the relevance of built-in information within dataset samples. A CNN architecture is then presented and tested with the constructed dataset. For various multipath parameter choices, experiments have demonstrated the detection performance of the proposed deep learning model. Further investigation using heatmaps provides additional understanding of the detection model decision rule and validates its relevance. The results provided in this PhD thesis are very encouraging and should motivate further research combining Machine Learning techniques and GNSS signal processing modelling. More specifically future research will continue the work initiated during the PhD aiming at generating the noise contribution at the correlator output by means of GANs instead of using pre-processed noise files. A focus should also be placed on multiple multipath that characterizes urban environment. Investigations will be conducted with deep regression architectures for multipath parameters estimation too. The time dynamic of the multipath should be studied as well in order to improve current static learning models. It should be noted that this PhD work is two-thirds complete but on hiatus following the departure of the candidate.

## 11. References

### 11.1 Link to PhD thesis / repository

The PhD thesis will not be available due to the departure of the candidate, but the code has been published:

- Blais A, Munin E, Couellan N. A synthetic GNSS correlator output generator. 2021, URL: [https://github.com/AntoineBlaisENAC/Synthetic\\_GNSS\\_Correlator\\_Output\\_Generator.git](https://github.com/AntoineBlaisENAC/Synthetic_GNSS_Correlator_Output_Generator.git).

### 11.2 Associated outputs and publications

- Evgenii Munin, Antoine Blais, Nicolas Couellan, "A Python code for GNSS signal generator", [http://github.com/EvgeniiMunin/gnss\\_signal\\_generator](http://github.com/EvgeniiMunin/gnss_signal_generator).

- Evgenii Munin, Antoine Blais, Nicolas Couellan, “Multipath detection at GNSS correlator output using image processing by convolutional neural network”, presented at the International Navigation Conference, Edinburgh, UK, November 2019.
- Evgenii Munin, Antoine Blais, Nicolas Couellan, “Convolutional neural network for multipath detection in GNSS receivers”, eprint, [arXiv:1911.02347](https://arxiv.org/abs/1911.02347), 2019.
- Evgenii Munin, Antoine Blais, Nicolas Couellan, “Multipath detection at GNSS correlator output using Convolutional Neural Networks”, article accepted and presented at the International Conference on Artificial Intelligence and Data Analytics for air Transportation (AIDA-AT/IEEE Computational Intelligence Society), Singapore, 3-4 feb 2020.
- Evgenii Munin, Antoine Blais, Nicolas Couellan, “GNSS multipath detection using embedded deep CNN on Intel® Neural Compute Stick”, presented at the Institute of Navigation conference GNSS+ 2020, Sept. 21-25 2020.
- Evgenii Munin, Antoine Blais, Nicolas Couellan, “A novel image representation of GNSS correlation for deep learning multipath detection”, ARRAY, Vol. 14, <https://doi.org/10.1016/j.array.2022.100167>. 2022.

### 11.3 References cited in this report

- [1] Van Dierendonck AJ, Fenton P, Ford T. Theory and performance of narrow correlator spacing in a GPS receiver. *Navigation* 1992;39(3):265–83.
- [2] Townsend B, Fenton P. A practical approach to the reduction of pseudorange multipath errors in a LI GPS receiver. In: *Proceedings of the 7th international technical meeting of the satellite division of the institute of navigation*. 1994, p.143–8.
- [3] Garin L, Rousseau J-M. Enhanced strobe correlator multipath rejection for code & carrier. In: *Proceedings of the 10th international technical meeting of the satellite division of the institute of navigation*. 1997, p. 559–68.
- [4] McGraw GA, Braasch MS. GNSS multipath mitigation using gated and high resolution correlator concepts. In: *Proceedings of the 1999 national technical meeting of the institute of navigation*. 1999, p. 333–42.
- [5] Jardak N, Vervisch-Picois A, Samama N. Multipath insensitive delay lock loop in GNSS receivers. *IEEE Trans Aerosp Electron Syst* 2011;47(4):2590–609.  
<http://dx.doi.org/10.1109/TAES.2011.6034653>.
- [6] Townsend B, Van Nee R, Fenton P, Van Dierendonck K. Performance evaluation of the multipath estimating delay lock loop. In: *Proceedings of the 1995 national technical meeting of the institute of navigation*. 1995, p. 277–83.
- [7] Zhang Y, Bartone C. Multipath mitigation in the frequency domain. In: *PLANS 2004. Position location and navigation symposium (IEEE Cat. No.04CH37556)*. 2004, p. 486–95.  
<http://dx.doi.org/10.1109/PLANS.2004.1309033>.
- [8] Zhang Y, Bartone C. Real-time multipath mitigation with WaveSmooth™ technique using wavelets. In: *Proceedings of the 17th international technical meeting of the satellite division of the institute of navigation*. 2004, p. 1181–94.
- [9] Vigneau W, Nouvel O, Manzano-Jurado M, Sanz C, Carrascosa AH, Roviras D, Juan JM, et al. Neural networks algorithms prototyping to mitigate GNSS multipath for LEO positioning applications. In: *Proceedings of the 19th international technical meeting of the satellite division of the institute of navigation*. 2006, p.1752–62.

- [10] Phan H, Tan S-L, Mcloughlin I, Vu L. A unified framework for GPS code and carrier-phase multipath mitigation using support vector regression. *Adv. Artif. Neural Syst.* 2013. <http://dx.doi.org/10.1155/2013/240564>.
- [11] Hsu L. GNSS multipath detection using a machine learning approach. In: *Proceedings of the 2017 IEEE 20th International conference on intelligent transportation systems.* 2017, p. 1–6. <http://dx.doi.org/10.1109/ITSC.2017.8317700>.
- [12] Suzuki T, Amano Y. NLOS multipath classification of GNSS signal correlation output using machine learning. *Sensors* 2021;21(7).
- [13] Quan Y, Lau L, Roberts G, Meng X, Zhang C. Convolutional neural network based multipath detection method for static and kinematic GPS high precision positioning. *Remote Sens* 2018;10(12). <http://dx.doi.org/10.3390/rs10122052>.
- [14] Schmidt E, Gatsis N, Akopian D. A GPS spoofing detection and classification correlator-based technique using the LASSO. *IEEE Trans Aerosp Electron Syst* 2020;56(6):4224–37. <http://dx.doi.org/10.1109/TAES.2020.2990149>.
- [15] Siemuri A, Kuusniemi H, Elmusrati MS, Välisuo P, Shamsuzzoha A. Machine learning utilization in GNSS—Use cases, challenges and future applications. In: *2021 International conference on localization and GNSS.* 2021, p. 1–6. <http://dx.doi.org/10.1109/ICL-GNSS51451.2021.9452295>.
- [16] Won J-H, Pany T. Signal processing. In: *Springer handbook of global navigation satellite systems.* Springer, Cham; 2017, p. 401–42. [http://dx.doi.org/10.1007/978-3-319-42928-1\\_14](http://dx.doi.org/10.1007/978-3-319-42928-1_14).
- [17] Kaplan ED, Hegarty CJ. *Understanding GPS: principles and applications.* 2<sup>nd</sup> ed. Artech House; 2006.
- [18] Ziedan NI. Improved multipath and NLOS signals identification in urban environments. *Navigation* 2018;65(3):449–62.
- [19] Blais A, Munin E, Couellan N. A synthetic GNSS correlator output generator. 2021, URL: [https://github.com/AntoineBlaisENAC/Synthetic\\_GNSS\\_Correlator\\_Output\\_Generator.git](https://github.com/AntoineBlaisENAC/Synthetic_GNSS_Correlator_Output_Generator.git).
- [20] Goodfellow I, Bengio Y, Courville A. *Deep learning.* MIT Press; 2016, <http://www.deeplearningbook.org>.
- [21] Shin H, Roth HR, Gao M, Lu L, Xu Z, Nogues I, et al. Deep convolutional neural networks for computer-aided detection: CNN architectures, dataset characteristics and transfer learning. *IEEE Trans Med Imaging* 2016;35(5):1285–98. <http://dx.doi.org/10.1109/TMI.2016.2528162>.
- [22] Voulodimos A, Doulamis N, Doulamis A, Protopapadakis E. Deep learning for computer vision: A brief review. *Comput Intell Neurosci* 2018;2018:1–13. <http://dx.doi.org/10.1155/2018/7068349>.
- [23] Simonyan K, Zisserman A. Very deep convolutional networks for large-scale image recognition. In: Bengio Y, LeCun Y, editors. *3rd International conference on learning representations, ICLR 2015, San Diego, CA, USA, May 7-9, 2015, Conference Track Proceedings.* 2015, URL: <http://arxiv.org/abs/1409.1556>.
- [24] Szegedy C, Vanhoucke V, Ioffe S, Shlens J, Wojna Z. Rethinking the inception architecture for computer vision. In: *2016 IEEE conference on computer vision and pattern recognition.* 2016, p. 2818–26. <http://dx.doi.org/10.1109/CVPR.2016.308>.
- [25] He K, Zhang X, Ren S, Sun J. Deep residual learning for image recognition. In: *2016 IEEE conference on computer vision and pattern recognition.* 2016, p.770–8. <http://dx.doi.org/10.1109/CVPR.2016.90>.

## Annex I: Acronyms

| <b>Term</b> | <b>Definition</b>                              |
|-------------|--|
| AI          | Artificial Intelligence                        |
| ATM         | Air Traffic Management                         |
| AWGN        | Additive White Gaussian Noise                  |
| C/A         | Coarse/Acquisition                             |
| C/N0        | Carrier-to-Noise ratio                         |
| CNN         | Convolutional Neural Network                   |
| CNS         | Communication, Navigation and Surveillance     |
| DLL         | Delay-Locked Loop                              |
| ENAC        | École Nationale de l'Aviation Civile           |
| GNSS        | Global Navigation Satellite System             |
| GPS         | Global Positioning System                      |
| LEO         | Low Earth Orbit                                |
| MEDLL       | Multipath Estimating Delay-Locked Loop         |
| NLOS        | Non-Line Of Sight                              |
| PRN         | Pseudo-Random Noise                            |
| PSD         | Power Spectral Density                         |
| SIGNAV      | SIGnal processing and NAVigation research team |
| VGG         | Visual Geometry Group                          |